



## OPEN ACCESS

## EDITED BY

Fernando Martinez-Rodrigo,  
University of Valladolid, Spain

## REVIEWED BY

Mohamed Salem,  
Universiti Sains Malaysia (USM), Malaysia  
Mohammad Tauquir Iqbal,  
Nanyang Technological University,  
Singapore

## \*CORRESPONDENCE

Bdereddin Abdul samad,  
abdulsamadbf@cardiff.ac.uk

## SPECIALTY SECTION

This article was submitted to Smart  
Grids,  
a section of the journal  
Frontiers in Energy Research

RECEIVED 27 June 2022

ACCEPTED 09 August 2022

PUBLISHED 15 September 2022

## CITATION

Karthikeyan B, Sundararaju K,  
Palanisamy R, Manivasagam R, Hossain I,  
Bajaj M, Shouran M, Abdul samad B and  
Kamel S (2022), A dual input single  
output non-isolated DC-DC converter  
for multiple sources electric  
vehicle applications.  
*Front. Energy Res.* 10:979539.  
doi: 10.3389/fenrg.2022.979539

## COPYRIGHT

© 2022 Karthikeyan, Sundararaju,  
Palanisamy, Manivasagam, Hossain,  
Bajaj, Shouran, Abdul samad and Kamel.  
This is an open-access article  
distributed under the terms of the  
[Creative Commons Attribution License  
\(CC BY\)](https://creativecommons.org/licenses/by/4.0/). The use, distribution or  
reproduction in other forums is  
permitted, provided the original  
author(s) and the copyright owner(s) are  
credited and that the original  
publication in this journal is cited, in  
accordance with accepted academic  
practice. No use, distribution or  
reproduction is permitted which does  
not comply with these terms.

# A dual input single output non-isolated DC-DC converter for multiple sources electric vehicle applications

B Karthikeyan<sup>1</sup>, K Sundararaju<sup>2</sup>, R Palanisamy<sup>3</sup>, R Manivasagam<sup>4</sup>,  
Ismail Hossain<sup>5</sup>, Mohit Bajaj<sup>6</sup>, Mokhtar Shouran<sup>7</sup>,  
Bdereddin Abdul samad<sup>7\*</sup> and Salah Kamel<sup>8</sup>

<sup>1</sup>Department of Electrical and Electronics Engineering, K. Ramakrishnan College of Technology, Trichy, India, <sup>2</sup>Department of Electrical and Electronics Engineering, M. Kumarasamy College of Engineering, Karur, India, <sup>3</sup>Department of Electrical and Electronics Engineering, SRM Institute of Science and Technology, Chennai, India, <sup>4</sup>Department of Electrical and Electronics Engineering, K. Ramakrishnan College of Engineering, Trichy, India, <sup>5</sup>School of Natural Sciences and Mathematics, Ural Federal University, Yekaterinburg, Russia, <sup>6</sup>Department of Electrical Engineering, Graphic Era (Deemed to be University), Dehradun, India, <sup>7</sup>School of Engineering, Cardiff University, Cardiff, United Kingdom, <sup>8</sup>Electrical Engineering Department, Faculty of Engineering, Aswan University, Aswan, Egypt

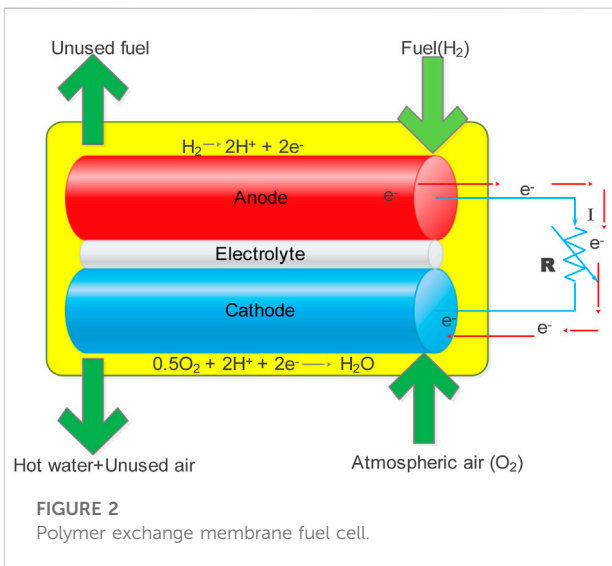
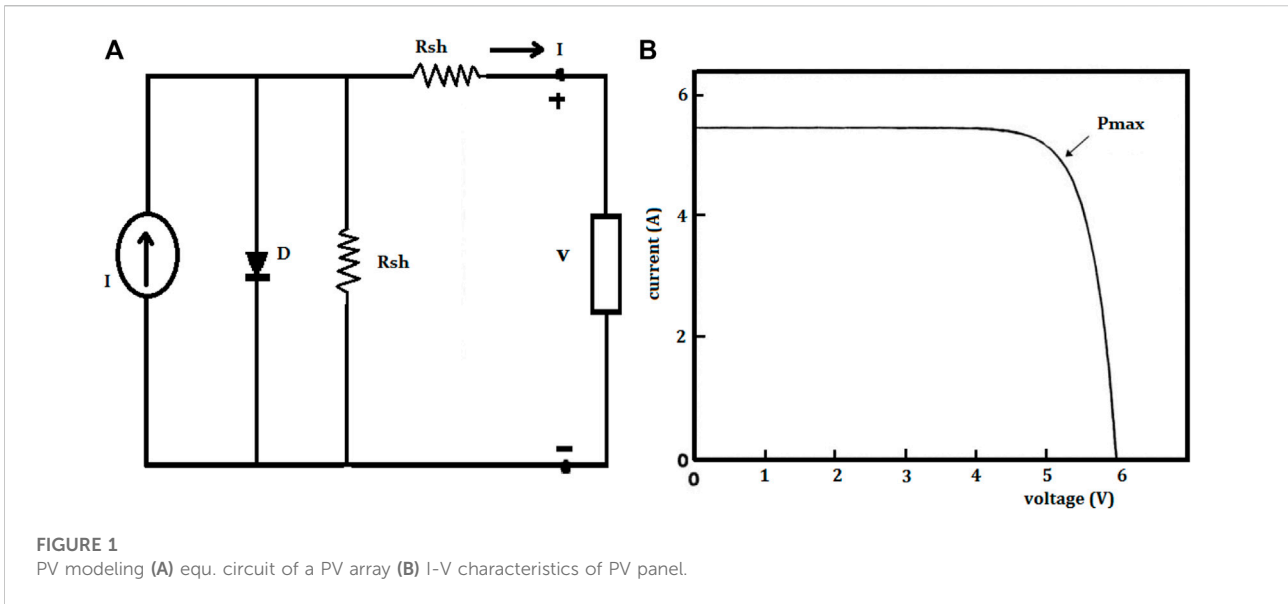
There is a need to design DC-DC converters capable of handling high voltages and that employ single-stage conversion to integrate renewable energy resources, such as solar photovoltaic cells and fuel cells, for electric vehicle applications. This paper elucidates the design and analysis of a dual input single output non-isolated Cuk-derived converter with a high step-up ratio. The proposed converter can effectively handle two different energy resources that have different electrical characteristics. It makes use of one common inductor between the dual input port, which reduces the passive components and the circuit volume required. The maximum efficiency that can be achieved by this converter is 95.72%, with two main switches and one diode in the circuit. This study involved a detailed analysis of the proposed converter in continuous current operation mode. A continuous current with reduced ripple in the output improves a fuel cell's operating life-span. The efficacy of the proposed converter is verified through simulation and validated by constructing a 200 W, real-time, scaled-down prototype model.

## KEYWORDS

non-isolated, dual input single output, high step up, multisource, electric vehicle

## 1 Introduction

The use of fossil fuels is undergoing a slow reduction, due to their finite nature and negative effects on the environment. Renewable sources of energy have the potential to meet demand without any adverse effects on the environment. Hence, it is an obvious choice to make use of renewable energy resources for power generation in grid-connected applications and for standalone automotive applications. Although there is a variety of



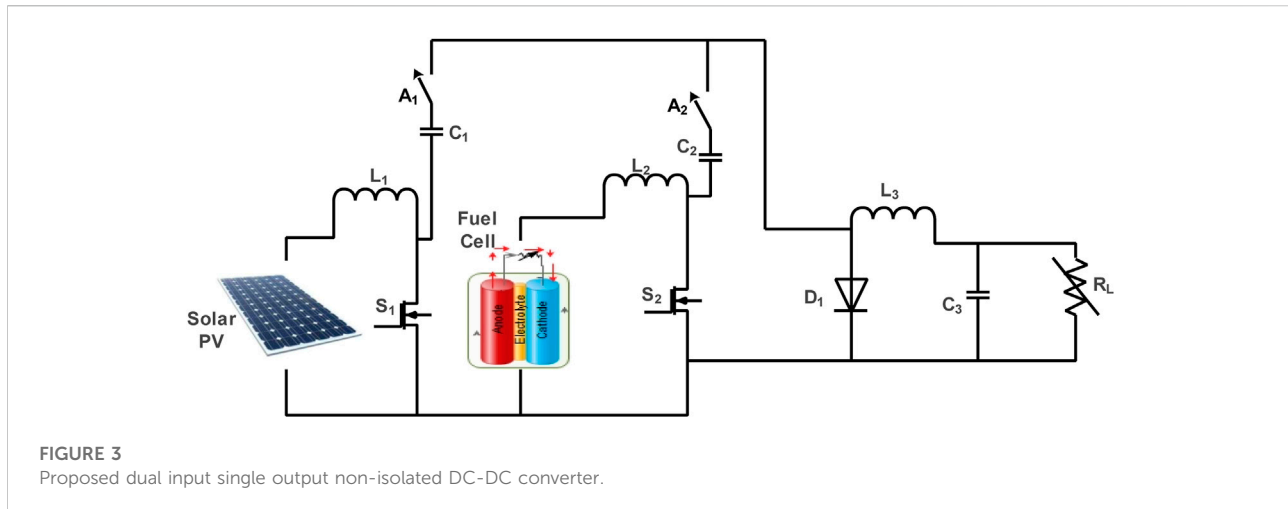
renewable energy resources available, solar photovoltaic (PV) and fuel cell sources possess advantages such as being portable and scalable in size. These advantages mean that these sources can be used for hybrid-source electric vehicle (HEV) applications. There is a crucial role for modern power electronics converters to address the issues while interconnecting with standalone automotive applications when it fed from renewable energy sources. In the remainder of this section, we review the extensive work carried by pioneering researchers in this field.

A multi-port non-isolated DC-DC converter was proposed by Suresh et al. (2021), which was capable of handling multiple energy sources. Their findings made it clear that the proposed

converter could perform step-up and step-down operations according to the load requirement, with an impressive voltage-conversion ratio and good power efficiency. A DC-DC converter topology for electric vehicle chargers was designed by Lee et al. (2019), which could achieve a power conversion efficiency of 97% and had high-speed charging capability. It had few passive components, resulting in a small circuit volume while achieving a high degree of energy density. A 20-kW experimental setup demonstrated the efficacy of their proposed converter.

For lithium-ion (Li-ion) batteries, super-capacitor powered HEV applications, a family of DC-DC converters were used by different researchers in the past. A review of various DC-DC converters for HEV applications, conducted by Mamouri et al. (2020), also stressed the importance of DC-DC converters for HEV applications. A multiple input port DC-DC converter with bidirectional capabilities, for use in HEV applications, was proposed by Akar et al. (2015). A simulation study of the battery and an ultracapacitor source demonstrated the good performance of the proposed converter. The experimental setup these researchers built could achieve an overall conversion efficiency of 93%, with minimum use of passive components.

For a wide range of input voltages, a powerful DC-DC converter design was essential in such a way it must be handling the hybrid energy sources. Taking this into consideration, a DC-DC converter was proposed by Hu et al. (2018). The proposed system was capable of handling two renewable sources, such as solar PV cells and wind energy, in complementary mode. The experimental arrangement demonstrated the accuracy of the modulation strategy in such a way that a smooth transition of the mode of operation occurred. Dusmez et al. (2015) designed a single input and multiple output DC-DC converter with zero voltage switching. Each cell in the proposed



topology comprised a resonant tank circuit which made the bulky circuit volume. The maximum power conversion efficiency achieved by this converter was almost 96% under a high-load current with reduced Duty cycle due to the use of soft switching capacity.

A single-input with dual-output DC-DC converter with buck/boost capability was proposed by [Shang and Wang \(2016\)](#). The proposed converter yielded a high voltage gain during the boost operation mode and achieved good steady state and dynamic characteristics during the buck operation mode. The switching losses were considerably reduced, resulting in improved efficiency. [Karthikeyan et al. \(2021\)](#) proposed a DC-DC converter topology dedicated for polymer exchange membrane (PEM) fuel cell applications, with switching pulses that were controlled by a fuzzy-based MPPT controller under variable temperature conditions. The proposed converter switches were triggered under zero voltage transition at medium to high power ranges. The simulation study and experimental results revealed the converter's capacity for handling fuel cell sources under variable temperature conditions.

It was difficult to handle much number of sources with individual DC-DC converters. Hence it could accomplish with the usage of Multiple-Input port and Multiple-Output port DC-DC converter designed by [Ahmed et al. \(2018\)](#). The research challenges faced by them during the analysis carried were also briefed by them. A detailed review of multiple-input and multiple-output DC-DC converters was carried out by [Dhanajaya et al. \(2021\)](#). The converters considered in the review were dedicated for grid-connected applications and HEV applications. The detailed review revealed the importance of multiple-input and multiple-output DC-DC converters.

A DC-DC converter was proposed by [Gupta et al. \(2020\)](#), with combined features of both Cuk converters and buck-boost converters, for renewable energy source integration with DC

micro-grid applications. The main advantage claimed in their work was minimum number stages without the aid of voltage multiplier cells and transformers. A single input and dual output solar powered DC-DC converter was proposed by [Akhil Raj and Arya \(2021\)](#), along with a modified P&O MPPT controller. The performances of the proposed converter were analyzed using the MATLAB Simulink tool and validated with the real time emulator, OP5142. A DC-DC converter with bidirectional capabilities for more than one source application was proposed by [Yi et al. \(2022\)](#). The proposed converter topology consisted of a minimum number of components and was able to charge/discharge the battery with minimum switching losses and improved peak efficiency.

A three-port DC-DC converter was proposed by [Aljarajreh et al. \(2021\)](#), in which two converters were bidirectional and one was unidirectional. In that study, generalized topological study to derive the three port converters among which two explicit bidirectional converters. A three-port DC-DC converter for simultaneously handling solar PV and battery sources was proposed by [Khoramikia et al. \(2018\)](#). The proposed converter incorporated a maximum power tracking controller for the solar PV system and a charging and discharging controller for the battery back-up. The voltage conversion gain was high enough to meet the demand by reducing the current ripples in the inductor and switching losses, thereby increasing the conversion efficiency.

## 2 Hybrid energy sources

### 2.1 Solar PV modeling

Solar energy is the most popular renewable source of energy in use because of its various features, such as silent operation,

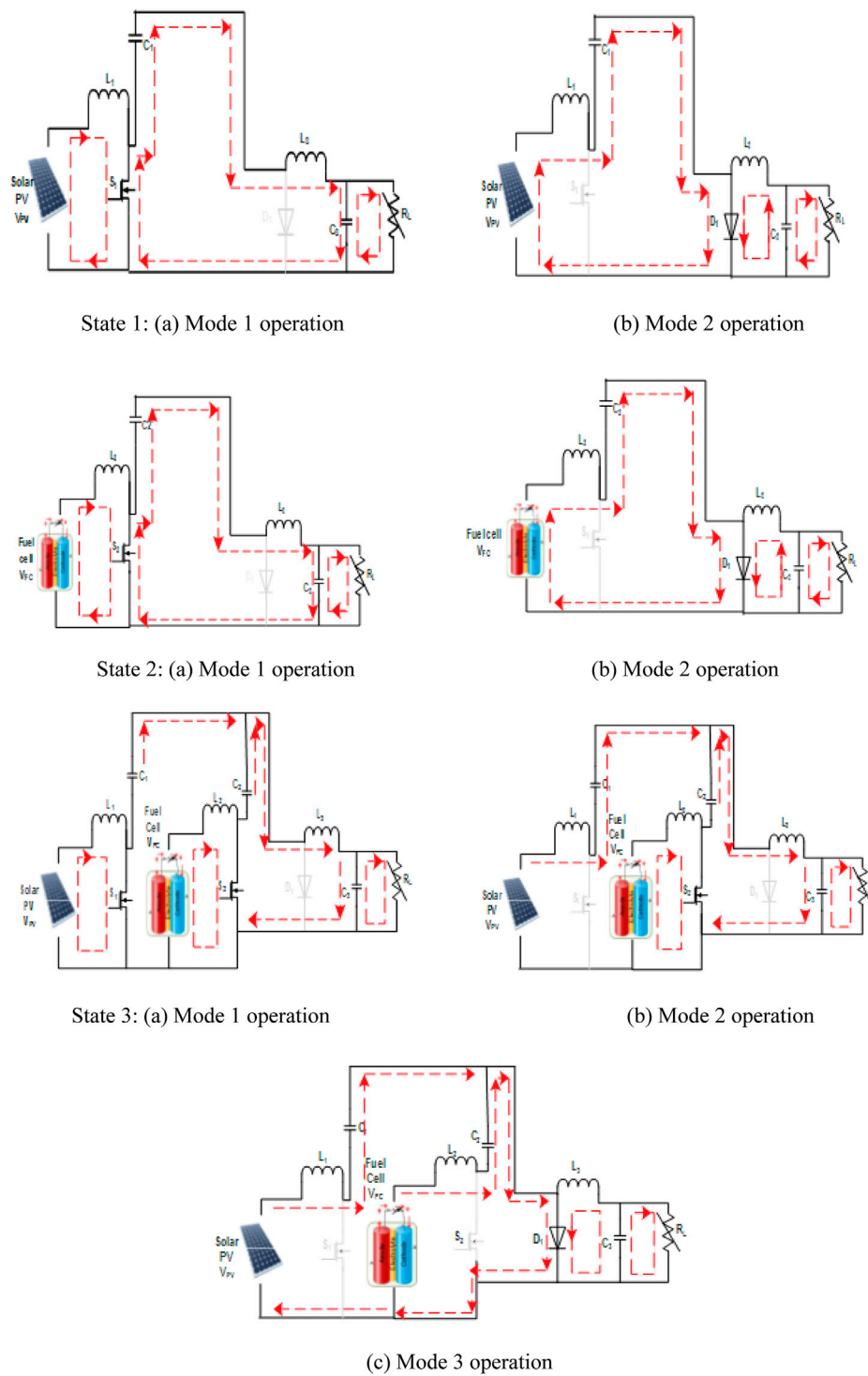
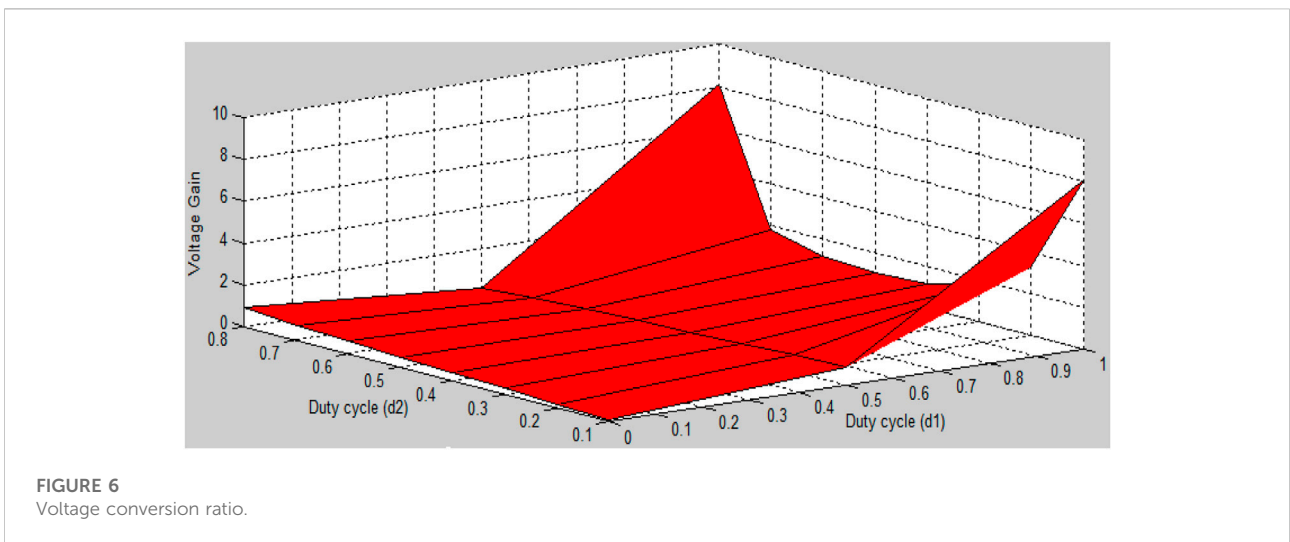
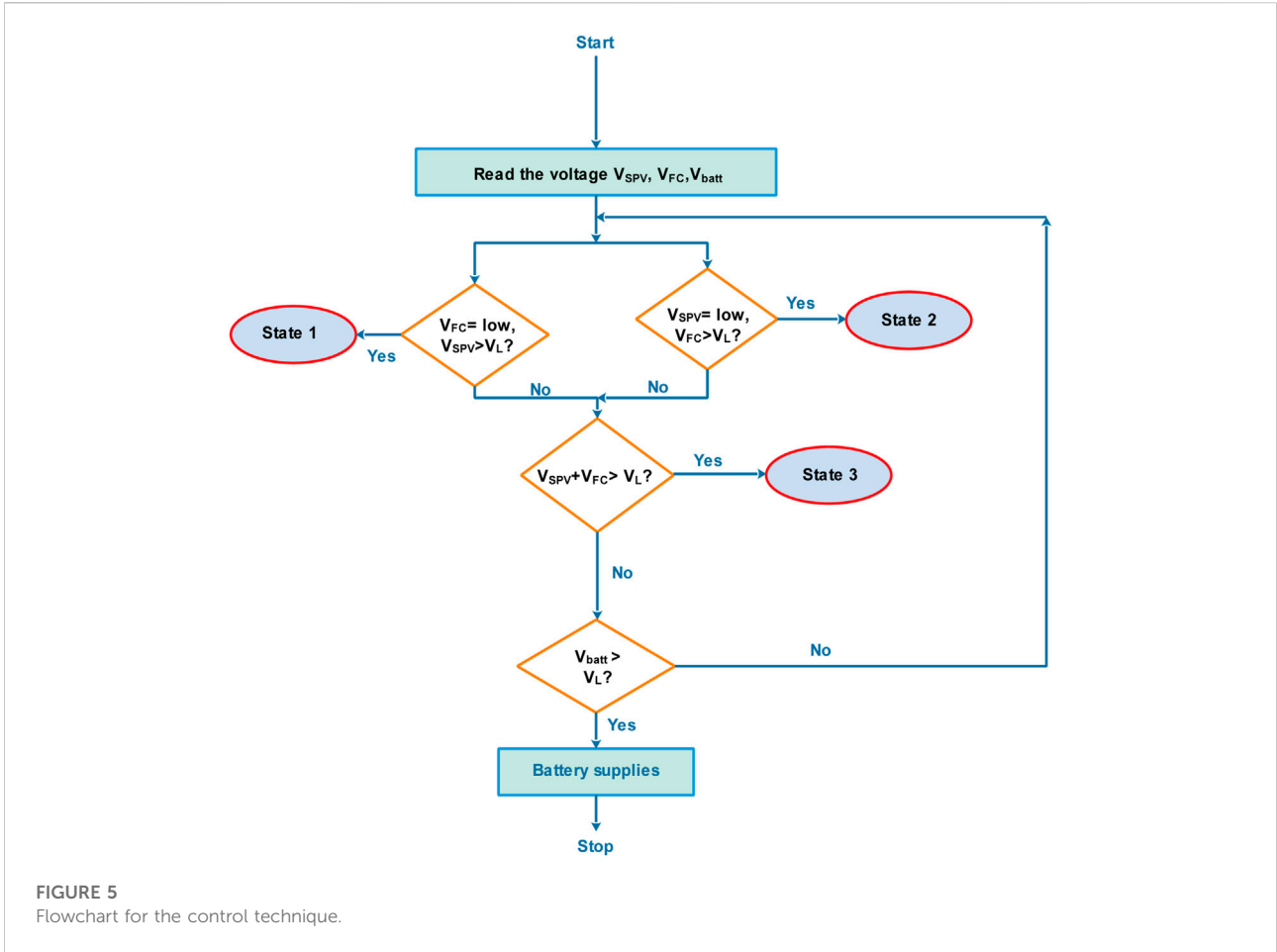


**FIGURE 4**

Mode of operation of the proposed DC-DC converter. State 1: (A) mode 1 operation (B) mode 2 operation. State 2: (A) mode 1 operation (B) mode 2 operation. State 3: (A) mode 1 operation (B) mode 2 operation (C) mode 3 operation.



being portable and scalable in size, quick start up etc. The conventional modeling of solar PV systems consists of a current source and a diode connected in anti-parallel across it.

The shunt resistance is extremely high in the parallel path and can be neglected in the modeling. The solar PV cells are connected in series and parallel to improve voltage and

TABLE 1 Components used in the proposed converter.

S.No	Components used	Symbol	Rating
1	Main switch	$S_1, S_2$	5 A
2	Auxiliary switch	$A_1, A_2$	2 A
3	Diode	$D_1$	5 A
4	Inductor	$L_1, L_2, L_3$	0.78 mH, 1.8 mH, 2 mH
5	Capacitor	$C_1, C_2, C_3$	46.5 $\mu$ F, 62.8 $\mu$ F, 2 $\mu$ F
6	Load resistance	$R_L$	100 $\Omega$

current levels, respectively. A solar array is made up of multiple PV cells connected in series and parallel. The parallel connection is responsible for increasing the current in the array, whereas the series connection is responsible for increasing the voltage of the module. The leakage current causes series resistance, whereas the impediment in the path of electron transport from the n to the p junction causes parallel resistance. Figure.1A illustrates the equivalent circuit for PV modeling.

The output current equations used to model a PV array are:

$$I = I_{sc} - I_d \tag{1}$$

$$I_d = I_g \left( e^{\frac{qV_d}{kT}} - 1 \right) \tag{2}$$

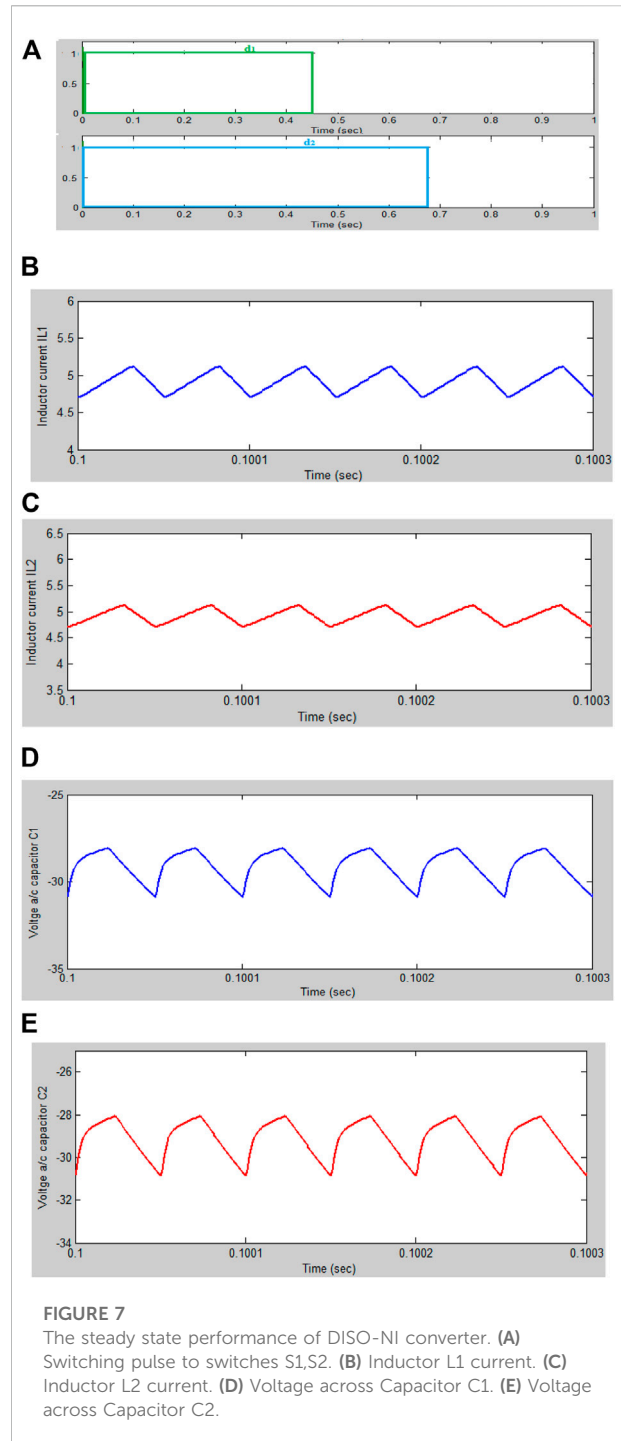
Where  $I_g$  is the diode’s reverse saturation current,  $n$  is the electron charge,  $V_k$  is the voltage across the diode,  $p$  is the Boltzmann constant, and  $T$  is the junction temperature. From Equations 1 and 2 we can obtain:

$$I = I_{sc} - I_g \left( e^{\frac{mV_k}{pT}} - 1 \right) \tag{3}$$

We could utilize two diode models to accurately model the solar panel, but our project’s topic of study was confined to the single diode model. Furthermore, the shunt resistance is very high and thus was overlooked during our research. Figure 1B demonstrates the I-V parameters of a typical solar cell.

### 2.2 Polymer exchange membrane fuel cell modeling

A fuel cell is an electrochemical device, in which chemical energy is directly converted into electrical energy. Fuel cells can be classified into many types depending on the material and nature of electrolyte is taken in the reformer. Among the types of fuel cells, PEM fuel cells play a vital role because of their major advantages, such as being scalable in size, having moderate power conversion efficiency, having a low operating temperature etc. Initially, the hydrogen-rich fuel is reformed in the reformer to produce pure hydrogen. This is oxidized into protons and electrons as indicated in the Figure 2. A proton is transferred from electrode “A” to



another electrode “B” through the PEM fuel cell, which strictly resists the electron flow. The electron will move from “A” to “B” through the external circuit, which causes an electric current. Oxygen-rich air is supplied at electrode “C” to enable reduction. The overall chemical reaction that takes place inside the fuel cell is shown in Figure 2.

The terminal voltage of a PEM fuel cell can be written as:

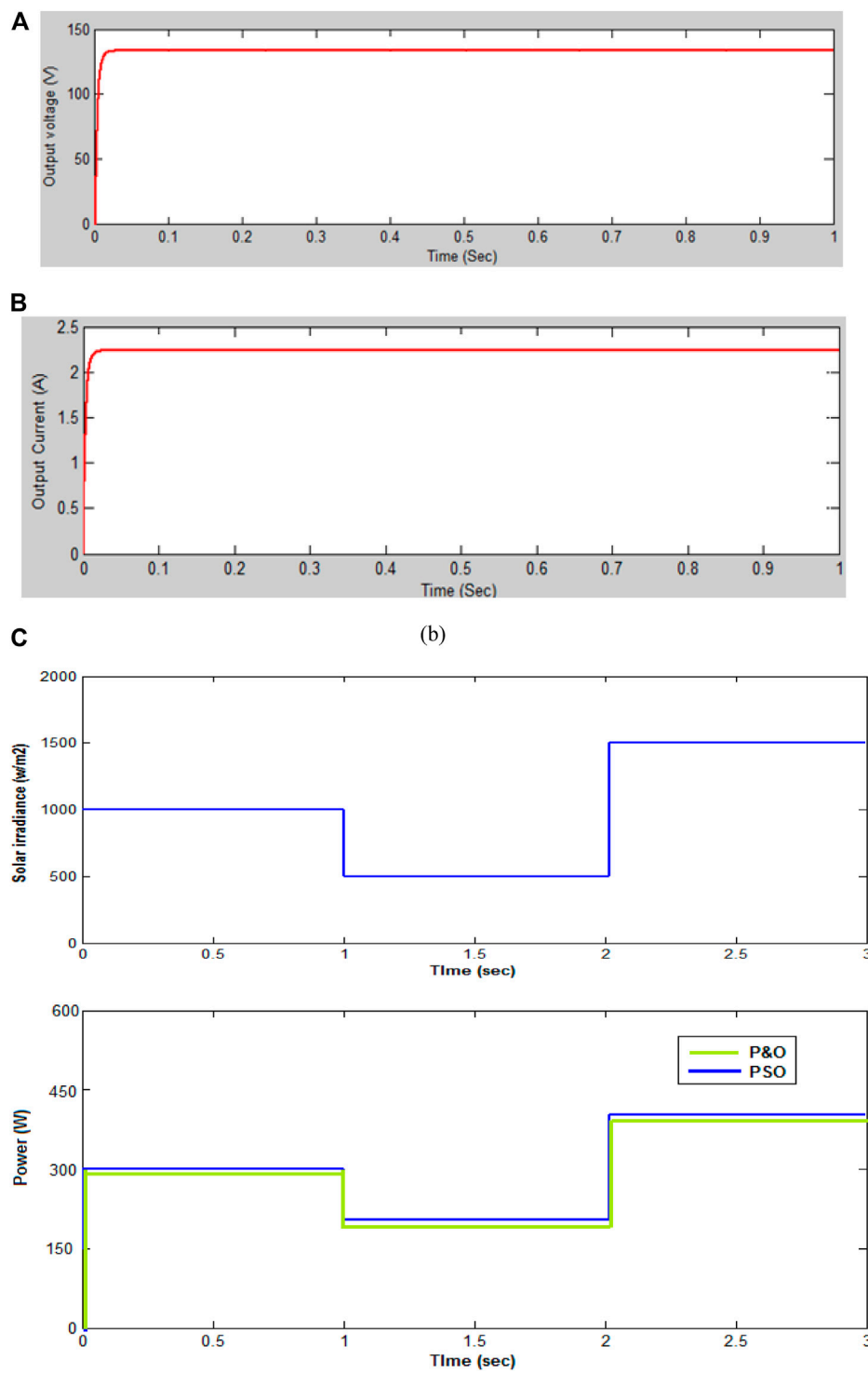


**FIGURE 8** (A) The output voltage of the dual input single output non-isolated converter fed by solar PV. (B) The output current of the dual input single output non-isolated converter fed by solar PV (C). The maximum power extracted from a solar PV using a PSO and a conventional P&O controller.

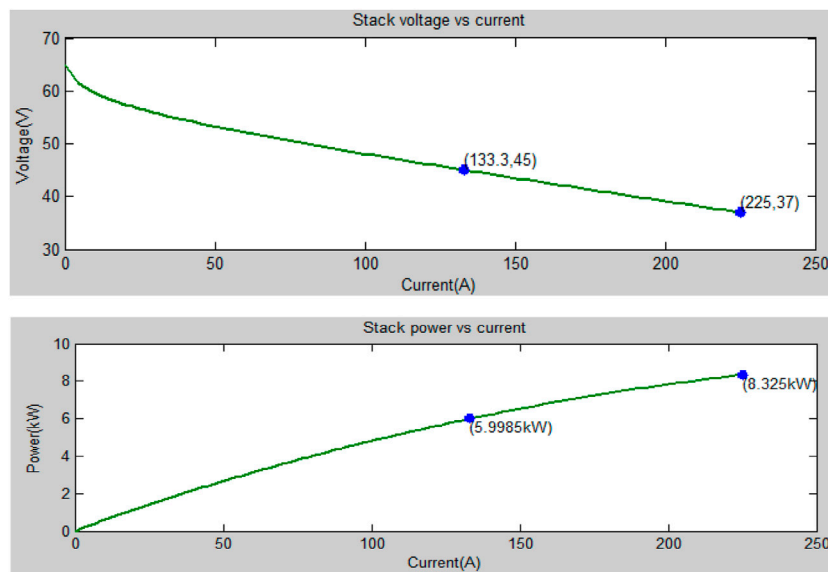


**FIGURE 9**  
Characteristics of a 6-kW PEM fuel cell.

$$V_{operating} = E_{ner} - \Delta V_R - \Delta V_{act} - \Delta V_{con} \quad (4)$$

According to Nernst’s equation:

$$E_{ner} = 1.2 - (8.5 \times 10^{-4})(T - 298.15) + (4.385 \times 10^{-5}T) \times \left[ \ln(P_{H_2}) + \frac{1}{2} \ln(P_{O_2}) \right] \quad (5)$$

where T is the operating cell temperature,  $P_{H_2}$  is the partial pressure of hydrogen, and  $P_{O_2}$  is the partial pressure of oxygen.

$$\Delta V_R = iR \quad (6)$$

where R is the total resistance of both the membrane and the contact and is expressed in ohms.

$$\Delta V_{act} = \delta_1 + \delta_2.T + \delta_3.T \ln(C_{O_2}) + \delta_4.T \ln(i) \quad (7)$$

$$\Delta V_{con} = \frac{-RT}{2F} \ln \left( 1 - \frac{i}{i_{max}} \right) \quad (8)$$

where R is the universal gas constant, F is Faraday’s constant, I is the fuel cell current, and  $i_{max}$  is the fuel cell current.

From Equations 1–5, it can be inferred that the operating voltage of PEM fuel cells depends on their operating parameters, such as cell temperature, hydrogen partial pressure, oxygen partial pressure, membrane water content, oxygen concentration etc.

### 3 The proposed non-isolated DC-DC converter

The proposed non-isolated DC-DC converter consists of two different renewable energy sources, such as a solar PV

system and a PEM fuel cell. It has two main switches ( $S_1, S_2$ ) and two auxiliary switches, as shown in Figure 3. The filter inductors ( $L_1, L_2$ ) remove current ripples and store electrical energy when the main switches are in the ON condition. The auxiliary switches are used to isolate either of the sources from the circuit if the other source is capable of delivering the energy to the load. There are is output inductor and capacitor combination ( $L_3-C_3$ ) to supply the load when main auxiliary diode  $D_1$  is in ON condition. To check the efficiency of the converter, a variable resistive load ( $R_L$ ) can be connected.

#### 3.1 Mode of operation

State 1:

In state 1, the auxiliary switch A1 is closed, whereas the auxiliary switch A2 is open, to ensure the solar PV is supplying the load. When switch  $S_1$  is in the ON condition, the inductor  $L_1$  is able to store energy. The diode  $D_1$  comes into action when the main switch  $S_1$  is in the OFF condition. The direction of the current during state 1 is shown in Figure 4 (state 1), and its steady state equations are derived as shown below.

$$V_{PV} = V_{L1} = L_1 \frac{di_1}{dt} \quad (9)$$

$$V_{L3} = \frac{1}{C_1} \int_{t_0}^{t_1} i(t) dt - \frac{1}{C_3} \int_{t_0}^{t_1} i(t) dt \quad (10)$$

$$i_{c1} = \frac{1}{L_3} \int (V_{c1} - V_{C3}) dt \quad (11)$$



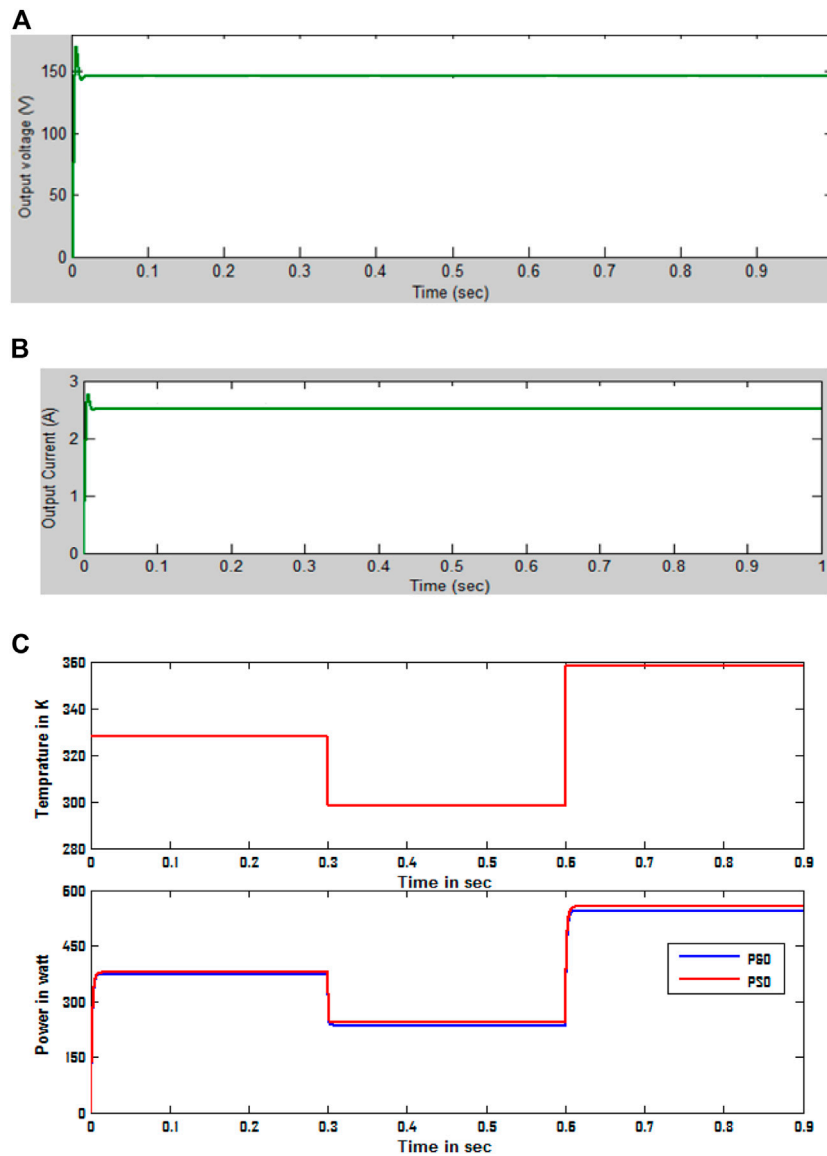


FIGURE 10

(A) The output voltage of the dual input single output non-isolated converter fed from a fuel cell (B) The output current of the dual input single output non-isolated converter fed from a fuel cell (C) The maximum power extracted from a PEM fuel cell using a PSO and a conventional P&O controller.

State 2:

The auxiliary switch  $A_2$  is closed to become connected with the fuel cell source, and auxiliary switch  $A_1$  is opened to disconnect the solar PV source, as shown in Figure 4 (state 2). The switch  $S_2$  is turned on, during which time the inductor  $L_2$  is being charged. The inductor is intended to release its stored energy when the main switch  $S_2$  is in the OFF condition and  $D_1$  is in the ON condition. The steady state equations of state 2 are derived as follows.

$$V_{FC} = V_{L2} = L_2 \frac{di_2}{dt} \tag{12}$$

$$V_{L3} = \frac{1}{C_2} \int_{t_0}^{t_1} i(t)dt - \frac{1}{C_3} \int_{t_0}^{t_1} i(t)dt \tag{13}$$

$$i_{c1} = \frac{1}{L_3} \int (V_{c2} - V_{C3})dt \tag{14}$$

$$G_v = -\frac{V_{RL}}{V_{PV}} \text{ (or)} -\frac{V_{RL}}{V_{FC}} \tag{15}$$

State 3:

When any one of the sources is not able to supply the load, it is necessary to use two sources simultaneously. In mode 1, both switches ( $S_1, S_2$ ) are turned on and both inductors ( $L_1,$

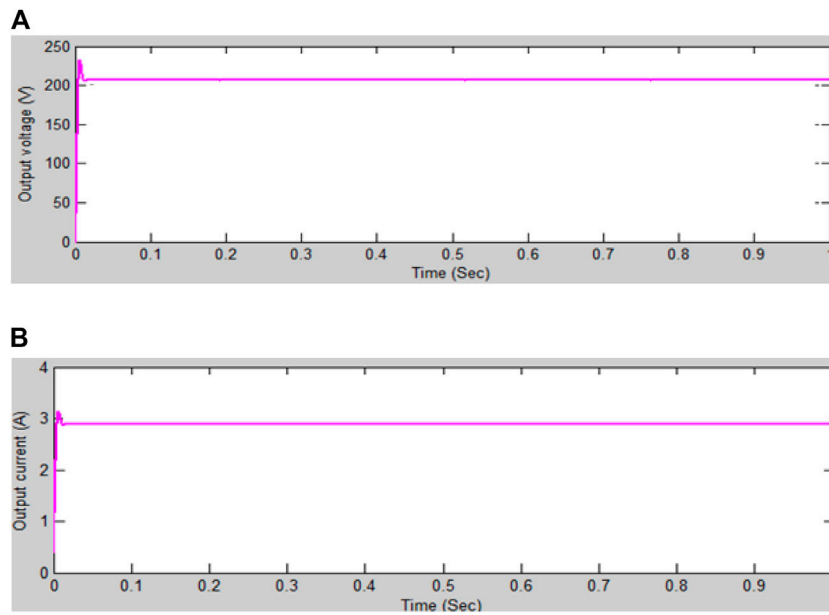


**FIGURE 11**  
**(A)** Output voltage of DISO-NI converter fed from Solar PV system and PEM fuel cell. **(B)** Output current of DISO-NI converter fed from Solar PV system and PEM fuel cell.

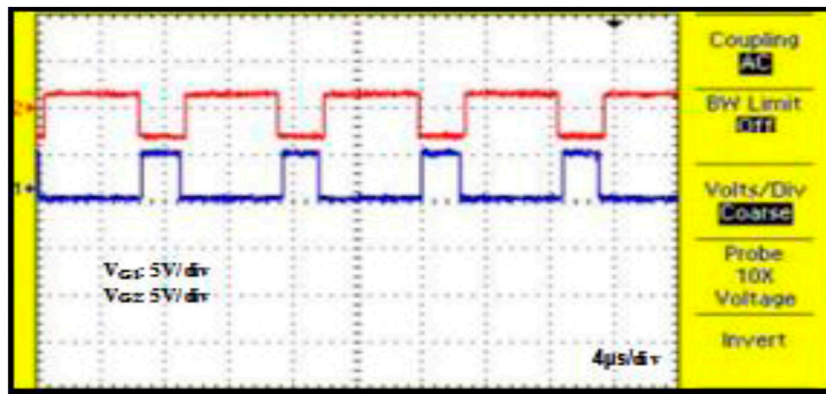


**FIGURE 12**  
 Switching pulses for the isolated DC-DC converter.

$L_2$ ) are being charged. The pre-charged capacitors ( $C_1$ ,  $C_2$ ) release energy to the load through the load-side inductor  $L_3$ .

$$i_{L3} = C_1 \frac{dV_{c1}}{dt} + C_2 \frac{dV_{c2}}{dt} \tag{16}$$

$$i_{RL} = i_{L3} + i_{C3} \tag{17}$$

During mode 2, the switch  $S_1$  is kept in the OFF condition, and the switch  $S_2$  is in the ON condition, which makes

the inductor current increase continuously. The energy stored in the inductor  $L_1$  is released to the capacitor  $C_1$  and the load-side inductor  $L_3$ , as shown in Figure 4 (state 3).

$$i_{PV} = i_{L1} = i_{C1} \tag{18}$$

$$i_{C1} = i_{C2} + i_{L3} \tag{19}$$

During mode 3, both switches are in the OFF condition, which makes the diode across the load to be in the ON

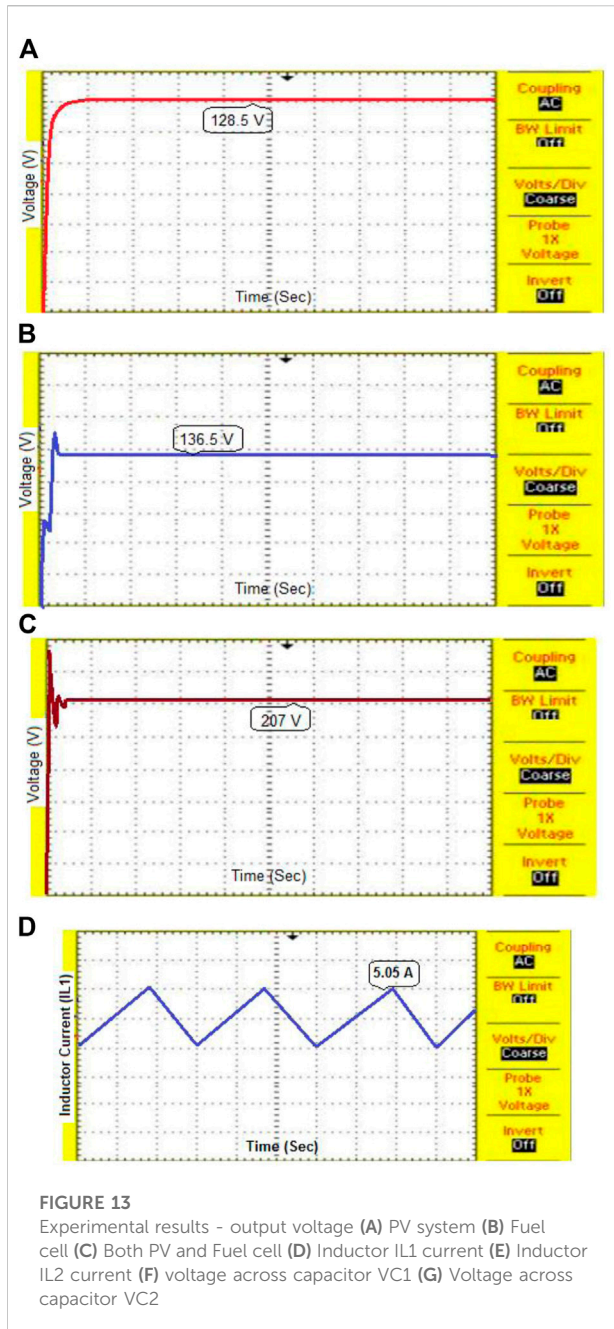


**FIGURE 13**  
Experimental results - output voltage (A) PV system (B) Fuel cell (C) Both PV and Fuel cell (D) Inductor IL1 current (E) Inductor IL2 current (F) voltage across capacitor VC1 (G) Voltage across capacitor VC2

condition. The solar PV voltage and stored energy in the inductor  $L_1$  are released through the capacitor  $C_1$ , while the fuel cell voltage and stored energy in the inductor  $L_2$  are released through the capacitor  $C_2$ , as shown in Figure 5. The load is free-wheeled through the diode  $D_1$ .

$$i_{PV} = i_{L1} = i_{C1} \text{ \& } i_{FC} = i_{L2} = i_{C2} \quad (20)$$

$$i_{C3} = i_{L3} - \frac{V_{Rt}}{R_L} \quad (21)$$

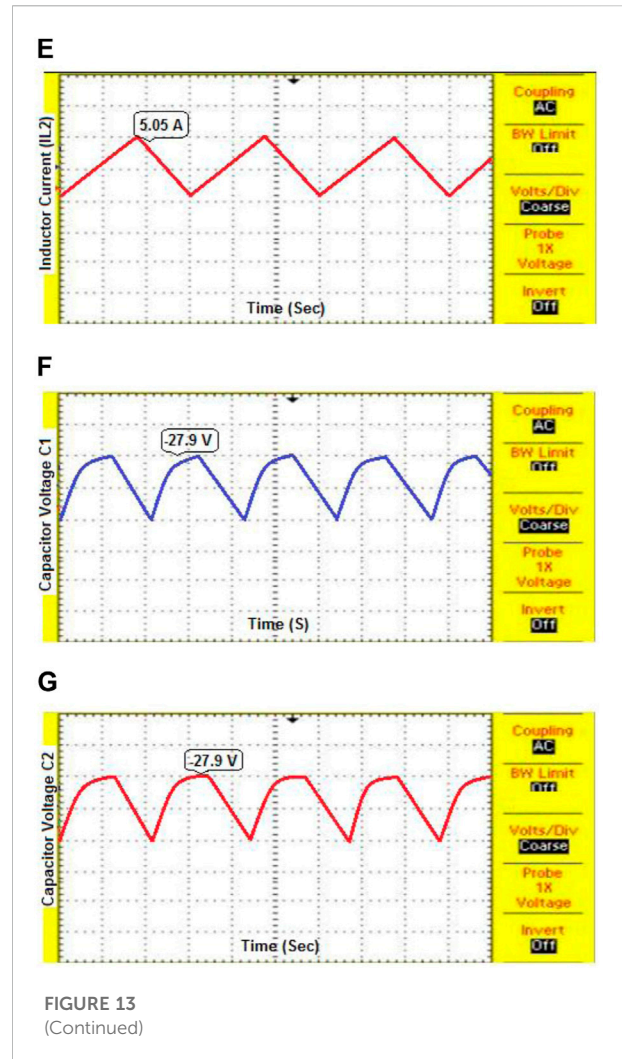


**FIGURE 13**  
(Continued)

## 4 Control strategies

The operating mode of the proposed double input single output non-isolated converter is shown in the flow diagram in Figure 5. Initially, the operating voltage of both the renewable energy sources and the battery are read by the controller. If the operating voltage of the solar PV system is higher than the demand, and the fuel cell is unable to meet the demand, then the solar PV is meant to deliver the load and the fuel cell is non-operative, and vice versa. If neither source is able to meet the demand individually but both sources combined are able to supply the load, then both sources are operated simultaneously. If both sources combined are unable to meet the demand, it is important to have a back-up source in place and ready to use.

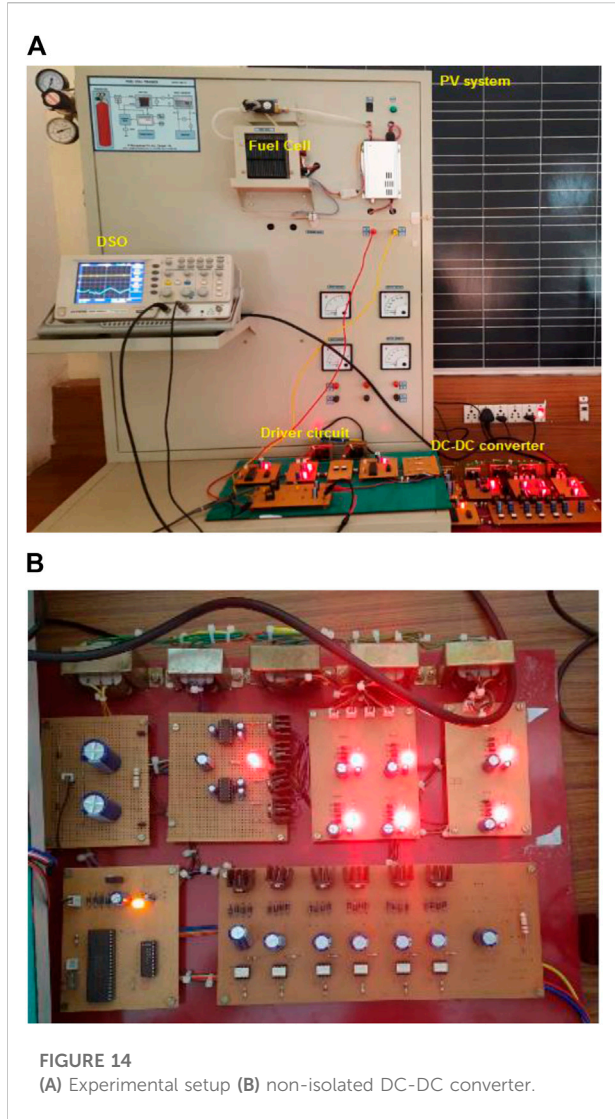


FIGURE 14 (A) Experimental setup (B) non-isolated DC-DC converter.

### 4.1 Particle swarm optimization (PSO)-based MPPT controller

It is essential to incorporate a maximum power tracking controller to trace the optimum power from solar panels and fuel cells under variable operating conditions. Modeling of solar PV systems has shown that the output voltage is influenced by many parameters, with solar irradiance being the most significant factor. Similarly, the fuel cell output voltage is influenced by many operating conditions, such as hydrogen pressure, membrane water content, concentration of the electrolyte, and temperature. Among these, temperature is considered to be the most significant. A common PSO algorithm-based maximum power tracking controller is designed in such a

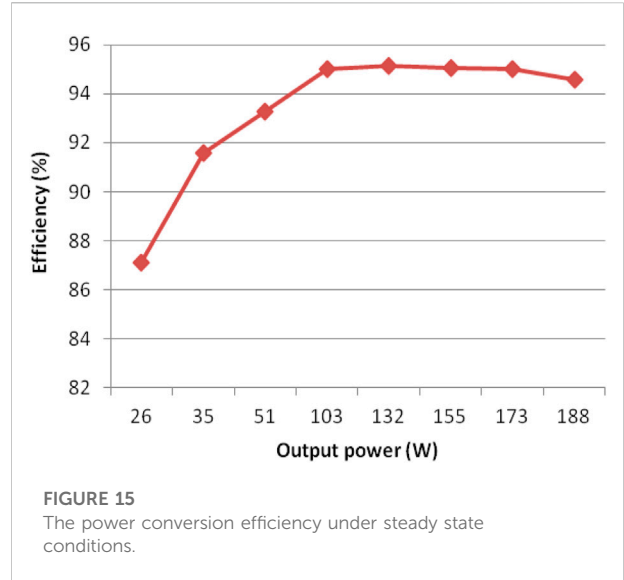


FIGURE 15 The power conversion efficiency under steady state conditions.

way that it ensures maximum power extraction from solar panels when solar irradiance varies and maximum power extraction from fuel cells when the operating temperature varies.

PSO is an evolutionary algorithm that imitates birds flocking while traveling from one place to another. It finds global maxima rather than local maxima. Each bird in a flock tries to find the optimum position ( $Y_i$ ) while traveling at certain velocity ( $\dot{x}_i$ ), represented as:

$$Y_i = (Y_{i1}, Y_{i2}, Y_{i3}, \dots, Y_{in})^T \tag{22}$$

$$\dot{x}_i = (\dot{x}_{i1}, \dot{x}_{i2}, \dot{x}_{i3}, \dots, \dot{x}_{in})^T \tag{23}$$

A previously visited position ( $P_v$ ) and the optimum previously visited position ( $P_{ov}$ ) are represented as:

$$P_v = (P_{v1}, P_{v2}, P_{v3}, \dots, P_{vn})^T \tag{24}$$

$$P_{ov} = (P_{ov1}, P_{ov2}, P_{ov3}, \dots, P_{ovn})^T \tag{25}$$

The particles are updated by multiplying the weight with the corresponding velocity, as shown below:

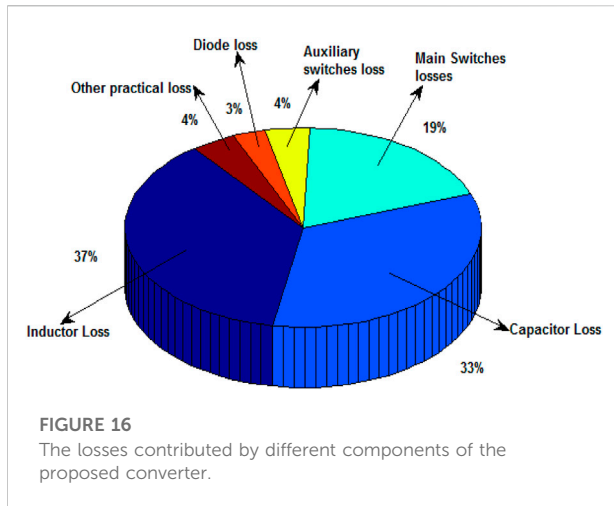
$$\dot{x}_{in} = (w \times \dot{x}_i) + a1c1(P_{vn} - Y_{in}) + a2c2(P_{ovn} - Y_{in}) \tag{26}$$

$$Y_{in} = Y_{in} + \dot{x}_{in} \tag{27}$$

Where  $i$  indicates the flock size,  $a_i$  represents the acceleration constant, and  $c_i$  represents random variables. The weight updating is performed in consecutive iterations, as follows:

$$w^n = w_{maximum} - \frac{(w_{maximum} - w_{minimum}) * n}{n_{max}} \tag{28}$$

$n_{max}$  represents the maximum iteration number, and  $n$  represents the iteration number.



### 4.2 Voltage conversion ratio

The total output voltage can be expressed as:

$$V_{output} = D_1V_{c1} + D_2V_{c2} \tag{29}$$

$$V_{FC} = (1 - D_2)V_{c2} \tag{30}$$

$$V_{PV} = (1 - D_1)V_{c1} + (D_2 - D_1)V_{c2} \tag{31}$$

From Equations 15 and 16, the total output voltage can be expressed as:

$$V_{output} = \frac{D_1}{(1 - D_1)}V_{PV} + \frac{(D_2^2 - D_1D_2)}{(1 - D_1)(1 - D_2)}V_{FC} \tag{32}$$

Figure 6 shows the voltage conversion ratio for the proposed system. Assuming an equal voltage is supplied by each of the renewable energy sources,  $V_{FC} = V_{PV} = V_{in}$ , the voltage conversion ratio is given by:

$$G_v = \frac{D_1}{(1 - D_1)} + \frac{(D_2^2 - D_1D_2)}{(1 - D_1)(1 - D_2)} \tag{33}$$

## 5 Small signal modeling

The proposed converter is excited from two different renewable energy resources and hence state space analysis is the obvious for small signal modeling (Iqbal and Maswood, 2020; Iqbal and Maswood, 2021). The transfer function of the n-dimensional system is given by:

$$\frac{C}{R} = C(SI - A)^{-1}B + D \tag{34}$$

where C and R represent the output and input of a converter, respectively, and A, B, C, and D represent a system matrix of (nxn), input matrix, output matrix, and transmission matrix, respectively. The generalized state model of any system can be described as follows:

$$\left. \begin{aligned} \frac{dX}{dt} &= AX + BU \\ Y &= CX + DU \end{aligned} \right\} \tag{35}$$

The selection of state variables and output variables is arbitrary and need not be unique. They can be chosen as follows:

$$X = \begin{bmatrix} i_{L1} \\ i_{L2} \\ i_{L3} \\ v_{C1} \\ v_{C2} \\ v_{C3} \end{bmatrix} \tag{36}$$

$$U = \begin{bmatrix} V_{PV} \\ V_{FC} \end{bmatrix} \tag{37}$$

$$Y = [V_{RL}] \tag{38}$$

TABLE 2 Performance comparison of various Cuk-derived converters.

S.No	Reference	No. of switches	No. of diodes	No. of capacitors	No. of inductors	Maximum power conversion efficiency	No. of ports
1	Suresh et al. (2021)	2	2	3	2	98.4%	4
2	Lee et al. (2019)	5	9	7	9	98.11%	2
3	Akar et al. (2015)	2	2	1	2	93%	3
4	Hu et al. (2018)	3	4	2	1	94.8%	3
5	Dusmez et al. (2015)	4	4	4	5	95.5%	3
6	Shang and Wang, (2016)	3	2	3	5	Not reported	3
7	Karthikeyan et al. (2021)	2	2	3	2	95.12%	2
8	Gupta et al. (2020)	2	8	3	5	Not reported	2
9	Aljarajreh et al. (2021)	4	3	5	5	98%	3
10	Proposed converter	4	1	3	3	95.72%	Extendable

The state model of the proposed converter can be formulated by referring to Equations 9 to 21, as follows:

$$\begin{bmatrix} \dot{i}_{L1} \\ \dot{i}_{L2} \\ \dot{i}_{L3} \\ v_{C1} \\ v_{C2} \\ v_{C3} \end{bmatrix} = \begin{bmatrix} 0 & 0 & 0 & \frac{-(1-D_1)}{L_1} & \frac{-(D_1-D_2)}{L_1} & 0 \\ 0 & 0 & 0 & 0 & \frac{-(D_2-1)}{L_2} & 0 \\ 0 & 0 & 0 & \frac{-D_1}{L_3} & \frac{-(D_1-D_2)}{L_3} & \frac{-1}{L_3} \\ \frac{-(1-D_1)}{L_1} & 0 & \frac{-D_1}{L_3} & 0 & 0 & 0 \\ \frac{(D_1-D_2)}{C_2} & \frac{D_2+1}{C_2} & \frac{D_1}{2C_1} + \frac{(D_2-D_1)}{C_2} & 0 & 0 & 0 \\ 0 & 0 & \frac{1}{C_3} & 0 & 0 & \frac{1}{RC_3} \end{bmatrix} \times \begin{bmatrix} i_{L1} \\ i_{L2} \\ i_{L3} \\ v_{C1} \\ v_{C2} \\ v_{C3} \end{bmatrix} + \begin{bmatrix} \frac{1}{L_1} & 0 \\ 0 & \frac{1}{L_2} \\ 0 & 0 \\ 0 & 0 \\ 0 & 0 \\ 0 & 0 \end{bmatrix} \begin{bmatrix} V_{PV} \\ V_{FC} \end{bmatrix} \tag{39}$$

$$\begin{bmatrix} V_{RL} \\ I_{RL} \end{bmatrix} = \begin{bmatrix} 0 & 0 & 0 & 0 & 0 & 1 \\ 0 & 0 & 0 & 0 & 0 & \frac{1}{R_L} \end{bmatrix} \begin{bmatrix} i_{L1} \\ i_{L2} \\ i_{L3} \\ v_{C1} \\ v_{C2} \\ v_{C3} \end{bmatrix} \tag{40}$$

### 5.1 Proportional integral (PI) controller tuning

To obtain a good steady-state performance, it is necessary to optimize the PI controller parameters. There are two parameters that must be calculated to achieve a good steady-state performance. These are the delay time and the time constant, the values of which must be optimized. The value of the delay time ( $D_{tp}$ ) and time constant ( $\tau_T$ ) are obtained using the Ziegler-Nichols method. Initially, the reaction curve is obtained using the Ziegler-Nichols method, through which both the parameters are obtained and substituted in Equation 34, which yields a significant reduction in the steady-state error (5.9%) and peak overshoot (58.12%).

$$G_C = K_p + \frac{K_i}{s} = K_p \left( 1 + \frac{1}{\tau_s} \right) \tag{41}$$

where  $K_p = \frac{0.878\tau_T}{D_{tp}}$  and  $\tau = \frac{D_{tp}}{0.3}$

## 6 Simulation results and discussion

The simulation analysis of the proposed converter for handling both solar PV and fuel cells was carried out using the MATLAB/R2022a Simulink environment. The components used in the simulation analysis and hardware setup are listed in

Table 1. The following section elucidates the simulation analysis with solar PV and fuel cell sources, and both sources simultaneously meet the demand.

### 6.1 Steady state simulation results

It is important to analyze the performance of the system with a fixed DC voltage under steady state conditions before it is supplied by two different renewable energy resources, each having different electrical characteristics. The duty cycles for the switches are maintained as  $d_1 = 0.45$  and  $d_2 = 0.68$ , as shown in Figure 7A. The corresponding inductor currents,  $I_{L1}$ ,  $I_{L2}$ , and the capacitor voltages,  $V_{C1}$  and  $V_{C2}$ , are shown in Figure 7B-E, which shows the variation in capacitor and inductor voltages to boost the applied DC input voltage.

Case 1: The solar PV can meet the demand

To analyze the performance of the proposed converter with a solar PV source, a 250 W, 40 V source is considered. In case 1), the solar PV alone is supplying the load. The input voltage received from the solar PV is 40 V. It is stepped-up to 130 V, and the output current obtained under this case is 2.32 A when the duty cycle is kept at  $d_1 = 76\%$ . The solar irradiance is varied as follows: 1,000  $w/m^2$  for 0–1 s, 500  $w/m^2$  for 1–2 s, and 1,500  $w/m^2$  for 2–3 s. The maximum power extracted from the solar panel with a P&O controller and a PSO controller is shown in Figure 8. The PSO controller outperformed the P&O controller in terms of maximum power and steady state performance.

To check the performance of the proposed converter with a PEM fuel cell source, a 6 kW, 45 V PEM fuel cell is considered, whose I-V and I-P are shown in Figure 9. In case 2), the solar PV is unable to supply the load so the fuel cell comes into action to supply the load. The open circuit voltage obtained was 45 V, as indicated in Figure 9. This increased to 146.25 V and the corresponding steady state current was 2.53 A when the duty cycle  $d_2 = 76.47\%$ , as shown in Figure 10. To check the performance of the PSO-based MPPT controller, the operating temperature of the fuel cell was varied as follows: 328 K for 0–0.3 s, 298 K for 0.3–0.6 s, and 358 K for 0.6–0.9 s. The corresponding power variation is shown in figure. The power extracted from a PEM fuel cell with a PSO controller was greater than the power extracted with a conventional P&O controller.

Case 3: The solar PV and fuel cell together are needed to meet the demand

Sometimes both sources are needed to meet the load if an individual source alone is unable to meet the load requirements. As a typical case, the solar PV supplies 30 V and the fuel cell supplies 35 V in case 3. The total voltage is increased to 211.25 V under steady state operating conditions when the duty cycle is kept at  $d_1 = 50\%$  and  $d_2 = 60\%$ , as shown in Figure 11.

## 7 Experimental results and discussion

An experimental setup was designed and used to test a dual input single output non-isolated Cuk-derived converter with a high step-up ratio, which provides better performance compared with other, conventional systems. This experimental setup included a PV system, a fuel cell, a non-isolated DC-DC converter, capacitors, and an inductor for boosting the voltage levels. The switching pulses are generated for a non-isolated DC converter using a PWM generator, which is shown in [Figure 12](#).

The overall converter losses were calculated to be 8.56%, which comprised the following losses: main switch loss, auxiliary switch loss, diode loss, inductor loss, capacitor loss, and other practical losses. The main and auxiliary switch losses included both switching and conduction losses.

The non-isolated DC-DC converter output voltage for the experimental system is shown in [Figure 13](#). [Figure 13A](#) shows the output voltage for the PV system operating as the input source, with a voltage of 128.5 V; similarly, [Figure 13B](#) shows the output voltage for the fuel cell operating as the input source, with a voltage of 136.5 V; while [Figure 13C](#) shows the output voltage for the PV system and the fuel cell operating together as the input source, with a voltage of 207 V. [Figure 13D–G](#) show the current flowing through the inductor and the voltage across the capacitors. The experimental setup of the proposed system is shown in [Figure 14](#). [Figure 15](#) illustrates the power conversion efficiency under steady state conditions. The losses due to the various components in the converter are shown in [Figure 16](#). [Table 2](#) shows a comparison of the performances of various Cuk-derived converters.

The number of main switches used in the proposed converter is two which are considerable less compared to all other converters used in the state of art. The auxiliary switches facilitate the integration of renewable energy sources depending upon the output voltage of source which is inevitable. Taking into account, the total switches considered to be four. Only one diode is used in the proposed converter, which is significantly fewer compared to the number of diodes used in all other converters reported in the literature. Three inductors and capacitors are used in the converter, which is compared against other converters as shown in [Table 2](#). The maximum conversion efficiency achieved by the proposed converter was 95.72%, which is significantly higher than some reported converters ([Mamouri et al., 2020](#); [Akar et al., 2015](#); [Hu et al., 2018](#); [Shang and Wang, 2016](#)), but slightly lower than some other converters ([Suresh et al., 2021](#); [Lee et al., 2019](#); [Ahmad et al., 2018](#)). The converters used by [Suresh et al. \(2021\)](#) and [Aljarajreh et al. \(2021\)](#) achieved a maximum efficiency of 98.4 and 98%, respectively, which operate in bidirectional mode. The converters used by [Suresh et al. \(2021\)](#) and [Aljarajreh et al. \(2021\)](#) achieved a maximum efficiency of 98.4 and 98%, respectively, which operate in bidirectional mode. The converter used by [Lee et al. \(2019\)](#) achieved a maximum efficiency of 98.11% which operate in unidirectional mode. It is evident that the maximum efficiency

of the proposed converter is optimum when operating in a unidirectional mode with the use of a non-isolated converter topology.

## 8 Conclusion

A dual input single output non-isolated DC-DC converter capable of handling multiple renewable sources of energy for electric vehicle applications was designed. The proposed converter was able to handle two renewable energy sources, such as a solar PV and a PEM fuel cell, that had different electrical characteristics. This converter was analyzed along with various operating control strategies, using MATLAB/R2021a Simulink environment under steady state and with two sources. The results showed that the performance of the proposed converter was superior to other state of the art converters. The hardware results were validated by constructing a 200-W experimental setup in the laboratory. The experimental results closely matched the simulation results, and showed that this converter is suitable for hybrid electric vehicle applications.

The highlights of this paper are listed below:

- ✓ The proposed converter was able to simultaneously handle two different renewable energy resources that had different electrical characteristics.
- ✓ The proposed converter made use of one common inductor between two input ports, which reduced the circuit volume and complexity.
- ✓ The proposed converter achieved a maximum power conversion efficiency of 95.31% under steady state conditions.

## Data availability statement

The original contributions presented in the study are included in the article/supplementary material; further inquiries can be directed to the corresponding author.

## Author contributions

All authors listed have made substantial, direct, and intellectual contributions to the work and approved it for publication.

## Conflict of interest

The authors declare that the research was conducted in the absence of any commercial or financial relationships that could be construed as a potential conflict of interest.

## Publisher's note

All claims expressed in this article are solely those of the authors and do not necessarily represent those of their affiliated

organizations, or those of the publisher, the editors and the reviewers. Any product that may be evaluated in this article, or claim that may be made by its manufacturer, is not guaranteed or endorsed by the publisher.

## References

- Ahmad, F., Haider, A. A., Naveed, H., Mustafa, A., and Ahmad, I. (2018). "Multiple input multiple output DC to DC converter," in 2018 5th International Multi-Topic ICT Conference (IMTIC) (Jamshoro, Pakistan: IEEE), 1–6.
- Akar, F., Tavlasoglu, Y., Ugur, E., Vural, B., and Aksoy, I. (2015). A bidirectional nonisolated multi-input DC–DC converter for hybrid energy storage systems in electric vehicles. *IEEE Trans. Veh. Technol.* 65 (10), 7944–7955. doi:10.1109/tvt.2015.2500683
- Akhil Raj, P., and Arya, S. R. (2021). Solar supplied two-output DC–DC converters in the application of low power. *Automatika* 62 (2), 172–186. doi:10.1080/00051144.2020.1805859
- Aljarajreh, H., Lu, D. D. C., Siwakoti, Y. P., Tse, C. K., and See, K. W. (2021). Synthesis and analysis of three-port DC/DC converters with two bidirectional ports based on power flow graph Technique. *Energies* 14 (18), 5751. doi:10.3390/en14185751
- Dhananjaya, M., and Pattnaik, S. (2021). *Review on multi-port DC–DC converters*. New Delhi, India: IETE Technical Review, 1–14.
- Dusmez, S., Khaligh, A., and Hasanzadeh, A. (2015). A zero-voltage-transition bidirectional DC/DC converter. *IEEE Trans. Ind. Electron.* 62 (5), 3152–3162. doi:10.1109/tie.2015.2404825
- Gupta, N., Almkhles, D., Bhaskar, M. S., Sanjeevikumar, P., Holm-Nielsen, J. B., and Mitolo, M. (2020). "Novel hybrid high gain converter: Combination of cuk and buck-boost structures with switched inductor for DC microgrid," in 2020 2nd Global Power, Energy and Communication Conference (GPECOM) (Izmir, Turkey: IEEE), 47–52.
- Hu, R., Zeng, J., Liu, J., and Yang, J. (2018). Double-input DC-DC converter for applications with wide-input-voltage-ranges. *J. Power Electron.* 18 (6), 1619–1626.
- Iqbal, M. T., and Maswood, A. I. (2020). "A frequency domain based large and small signal modeling of three phase dual active bridge," in IECON 2020 The 46th Annual Conference of the IEEE Industrial Electronics Society, 3421–3426. doi:10.1109/IECON43393.2020.9254773
- Iqbal, M. T., and Maswood, A. I. (2021). An explicit discrete-time large- and small-signal modeling of the dual active bridge DC–DC converter based on the time scale methodology. *IEEE J. Emerg. Sel. Top. Ind. Electron.* 2 (4), 545–555. doi:10.1109/JESTIE.2021.3087942
- Karthikeyan, B., Sundararaju, K., and Palanisamy, R. (2021). A variable step size fuzzy logic controller based maximum power point tracking controller for proton exchange membrane fuel cell powered resonant pulse width modulation high step up converter with multicarrier sinusoidal pulse width modulation inverter fed induction motor. *Int. Trans. Electr. Energy Syst.* 31 (11). doi:10.1002/2050-7038.13093
- Khoramikia, H., Heydari, M., and Dehghan, S. M. (2018). "A new three-port non-isolated DC-DC converter for renewable energy sources application," in Electrical Engineering (ICEE), Iranian Conference on (Mashhad, Iran: IEEE), 1101–1106.
- Lee, W. S., Kim, J. H., Lee, J. Y., and Lee, I. O. (2019). Design of an isolated DC/DC topology with high efficiency of over 97% for EV fast chargers. *IEEE Trans. Veh. Technol.* 68 (12), 11725–11737. doi:10.1109/tvt.2019.2949080
- Mamouri, L., Mesbahi, T., Bartholomeus, P., and Théophile, P. A. U. L. (2020). "Design of a DC/DC power converter for Li-ion battery/supercapacitor hybrid energy storage system in electric vehicles," in 2020 IEEE Vehicle Power and Propulsion Conference (VPPC) (Gijon, Spain: IEEE), 1–5.
- Shang, M., and Wang, H. (2016). "A ZVS integrated single-input-dual-output DC/DC converter for high step-up applications," in 2016 IEEE Energy Conversion Congress and Exposition (ECCE) (Milwaukee, WI, USA: IEEE), 1–6.
- Suresh, K., Bharatiraja, C., Chellammal, N., Tariq, M., Chakraborty, R. K., Ryan, M. J., et al. (2021). A multifunctional non-isolated dual input-dual output converter for electric vehicle applications. *IEEE Access* 9, 64445–64460. doi:10.1109/access.2021.3074581
- Yi, W., Ma, H., Peng, S., Liu, D., Ali, Z. M., Dampage, U., et al. (2022). Analysis and implementation of multi-port bidirectional converter for hybrid energy systems. *Energy Rep.* 8, 1538–1549. doi:10.1016/j.egy.2021.12.068